Journal of Electron Devices, Vol. 13, 2012, pp. 960-964

© JED [ISSN: 1682 -3427]

Journal of Electron Devices
www.jeldev.org

EFFECT OF PACKAGE PARASITICS ON THE MILLIMETER-WAVE PERFORMANCE OF DDR SILICON IMPATT DEVICE OPERATING AT W-BAND

Aritra Acharyya[1,*], Suranjana Banerjee[2], and J. P. Banerjee[3]

[1,3]Institute of Radio Physics and Electronics, University of Calcutta, 92, APC Road, Kolkata - 700009, India.

[2]Academy of Technology, West Bengal University of Technology, Adisaptagram, Hooghly 712121, West Bengal, India

ari_besu@yahoo.co.in[1,*]

Received 22-02-2012, accepted 06-03-2012, online 07-03-2012

ABSTRACT

The effect of package parasitics on the millimeter-wave performance of double drift region (DDR) Silicon IMPATT device operating at W-band is studied in this paper. A lumped equivalent circuit of the W-band IMPATT source is considered and the effect of package parasitics on the high-frequency performance of the device is investigated using a generalized double-iterative computer method based on drift-diffusion model. Results show that the high-frequency parameters such as device peak negative conductance, peak optimum frequency, RF power output are decreased significantly when the device is packaged into the W-band (*75 GHz – 110 GHz*) package. For example, the output RF power density of the device decreased by *32.5 %* due the effect of parasitic inductance and parasitic capacitance introduced by the package.

Keywords: Package parasitics, Millimeter-wave, DDR IMPATT, Series resistance.

I. INTRODUCTION

Impact Ionization Avalanche Transit Time (IMPATT) diodes have emerged as the most efficient among other solid state sources to deliver high power at millimeter-wave and sub-millimeter wave frequencies [1-3]. The rapid development of silicon technology in the decade of seventies has made possible the practical realization of Si single drift (SDR) and double drifts (DDR) IMPATTs capable of providing RF output power of the order of several watts at mm-wave frequency bands [4-5]. Generally the package associated with a millimeter-wave IMPATT is very much crucial in determining the overall device performance. The parasitic inductance and capacitance introduced by the package degrade the performance of the device by forcing the diode to operate at lower optimum design frequency and degrade the overall diode quality factor.

In the present paper, the authors have studied the effect of package parasitics on the overall RF performance of the DDR Si IMPATT device operating at W-band. A generalized double iterative computer method based on drift-diffusion model is used to study the DC and small-signal parameters of a DDR Si IMPATT device designed to operate at *94 GHz* window frequency. Effect of package parasitics on the RF performance of the device is investigated by using a lumped equivalent circuit of the W-band IMPATT source as discussed in section III. Results obtained from the simulation are discussed in section IV. Finally the paper is concluded in section V.

II. DESIGN AND SIMULATION TECHNIQUE

The frequency of operation of an IMPATT diode essentially depends on the transit time of charge carriers to cross the depletion layer of the diode. IMPATT diodes having symmetrical double drift p^+pnn^+ structure are first designed for a particular design frequency (f_d) by using computer simulation technique and the transit time formula of Sze and Ryder [6] given by $W_{n,p} = 0.37\, v_{sn,sp} / f_d$; where $W_{n,p}$ and $v_{sn,sp}$ are the *n* or *p*-side depletion layer width, saturation velocity of electrons/holes respectively. Here n^+ and p^+-layers are highly doped substrates whose doping concentrations are taken to be $10^{26}\ m^{-3}$. The background doping concentrations of *n* and *p* - depletion regions are initially chosen according to the design frequency. The electric field profile using the above doping profile is obtained from the DC simulation [7]. The input doping profile is adjusted so that the electric field just punches through the depletion layers ($W_{n,p}$) for a particular value of f_d and a particular biasing current density J_0. Small-signal computer simulation [8] based on Gummel-Blue approach [9] is then carried out to obtain the admittance characteristics of the device. The optimum frequency (f_p) for peak negative conductance is determined from the admittance characteristics. If the magnitude of f_p differs very much from f_d, the value of J_0 is varied and the computer simulation program is run till the value of f_p is nearly equal to the value of f_d. The bias current density is thus fixed for the particular design frequency. Realistic doping profile for flat profile diode has been used for the present analysis. The doping profile at the interfaces of epitaxy and substrate are approximated as error function. The doping profile near the metallurgical junction has been made realistic by suitable exponential functions.

A Si based DDR IMPATT device is designed and optimized for CW operation at *94 GHz* window frequency following the above said design methodology. The design parameters are listed in Table 1.

One-dimensional model of reverse biased p^+pnn^+ structure as shown in Figure 2 is taken for DC and small-signal analysis of DDR IMPATT device. The DC electric field and current density profiles in the depletion layer of the device are obtained from simultaneous numerical solution of

fundamental device equations i.e., Poisson's equation, combined carrier continuity equation in the steady state, current density equations and mobile space charge equation [10-11] subject to appropriate boundary conditions. A double iterative, field maximum simulation method based on Gummel-Blue approach [9] described elsewhere [7] is used to solve these equations and obtain the field and current density profiles. The magnitude of peak field at the junction (ξ_m), the widths of avalanche and drift zones (x_A and x_D; where $x_D = d_n + d_p$) and the voltage drops across these zones (v_A, v_D) are obtained from double iterative simulation program. These values are fed back as input parameters in the small-signal simulation of the admittance properties of the device. The depletion layer edges of the device obtained from the output of DC simulation program are taken as the starting and end points of numerical computation in the small-signal program. Two second order differential equations are framed by resolving the diode impedance $Z(x,\omega)$ into its real part $R(x,\omega)$ and imaginary part $X(x,\omega)$; where, $Z(x,\omega) = R(x,\omega) + jX(x,\omega)$. Under small-signal condition the differential equations involving negative specific resistance R and specific reactance X are given by [8],

$$D^2R+\left[\alpha_n(x)-\alpha_p(x)\right]DR-2\underline{r}\left(\frac{\omega}{\underline{v}}\right)DX+\left[\left(\frac{\omega^2}{\underline{v}^2}\right)-H(x)\right]R- 2\underline{\alpha}(x)\left(\frac{\omega}{\underline{v}}\right)X-2\left(\frac{\underline{\alpha}(x)}{\underline{v}\varepsilon}\right)=0 \quad (1)$$

$$D^2X+\left[\alpha_n(x)-\alpha_p(x)\right]DX+2\underline{r}\left(\frac{\omega}{\underline{v}}\right)DR+\left[\left(\frac{\omega^2}{\underline{v}^2}\right)-H(x)\right]X+ 2\underline{\alpha}(x)\left(\frac{\omega}{\underline{v}}\right)R+\left(\frac{\omega}{\underline{v}^2\varepsilon}\right)=0 \quad (2)$$

Where the following notations have been introduced, $\underline{v}=\left(v_{sp}v_{sn}\right)^{0.5}$, $\underline{\alpha}(x)=\left(\alpha_p(x)v_{sp}+\alpha_n(x)v_{sn}\right)/2\underline{v}$, $\underline{r}=\left(v_{sn}-v_{sp}\right)/2\underline{v}$, $H(x)=\left(J_0/\underline{v}\varepsilon\right)\left[2d\underline{\alpha}/d\xi+y.d\left(\alpha_n-\alpha_p\right)/d\xi\right]$, $H(x)$ is the linearization factor. $y=\underline{v}\varepsilon/J_0\left(d\xi_m/dx\right)$, ε = Permittivity of the semiconductor, D is the differential operator $\partial/\partial x$. The boundary conditions for R and X at the n^+n and p^+p interfaces are given by,

$$DR+\frac{\omega X}{v_{sn}}=-\left(\frac{1}{v_{sn}\varepsilon}\right) \;\&\; DX-\frac{\omega R}{v_{sn}}=0$$

at $x = -x_1$ i.e., at n^+n interface (3)

$$DR-\frac{\omega X}{v_{sp}}=\left(\frac{1}{v_{sp}\varepsilon}\right) \;\&\; DX+\frac{\omega R}{v_{sp}}=0$$

at $x = x_2$ i.e., at p^+p interface (4)

A double-iterative simulation over the initial choice of the values of R and X described in details in [10] is used to solve simultaneously the two second order differential equations (1) and (2) in R and X subject to appropriate boundary conditions expressed in equations (3) and (4). The negative resistivity ($R(x)$) and reactivity ($X(x)$) profiles are obtained from the above solution. The device negative resistance (Z_R) and reactance (Z_X) are obtained from the numerical integration of the $R(x)$ and $X(x)$ profiles over the space-charge layer width, W. Thus,

$$Z_R=\int_{-x_1}^{x_2}R(x)dx \;\&\; Z_X=\int_{-x_1}^{x_2}X(x)dx \quad (5)$$

The impedance of the device is given by, $Z_D = Z_R + j\,Z_X$ and the device admittance is, $Y_D = 1/Z_D = G + j\,B$. The negative conductance ($-G$) and positive susceptance (B) are computed from the following expressions,

$$\left|G(\omega)\right|=\frac{Z_R}{\left(Z_R{}^2+Z_X{}^2\right)} \;\&\; \left|B(\omega)\right|=\frac{-Z_X}{\left(Z_R{}^2+Z_X{}^2\right)} \quad (6)$$

It may be noted that both $-G$ and B are normalized to the area of the diode. The admittance ($G(\omega)$ versus $B(\omega)$) plots of the device can be obtained for different bias current densities from the above analysis. At a resonant frequency of oscillation, the maximum RF power output (P_{RF}) from the device can be obtained from the following expression,

$$P_{RF}=\frac{1}{2}.V_{RF}^2.\left|-G_p\right|.A_j \quad (7)$$

Where, V_{RF} is the amplitude of the RF swing ($V_{RF} = V_B/2$, assuming *50%* modulation of the breakdown voltage V_B), $-G_p$ is the diode negative conductance at the operating frequency and A is the junction area of the diode ($A_j = \pi(D/2)^2\ m^2$, where $D = 35\ \mu m$ (junction diameter) [4-5] for CW operation). The DC and Small-signal simulation method of IMPATT devices presented in the paper is free from simplified assumptions and it takes into account the realistic doping profiles, recently reported values of material parameters [12-14] at *500 K* and the effect of mobile space charge [10-11].

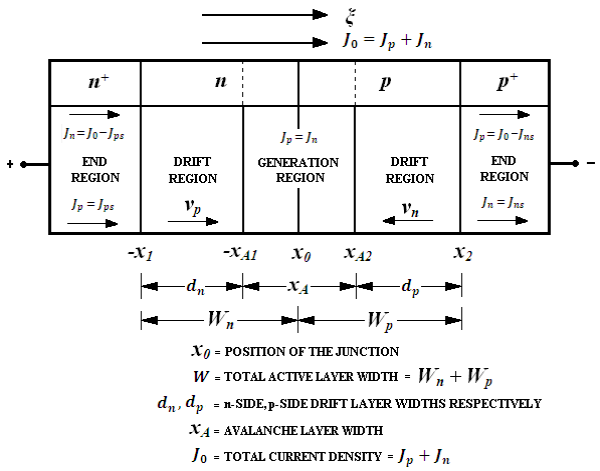

Figure 1: One-dimensional model of DDR IMPATT device.

III. LUMPED EQUIVALENT CIRCUIT OF THE W-BAND IMPATT SOURCE

An equivalent circuit representation of IMPATT device with package and RF load is shown in Figure 2 [15], where G and B are the diode conductance and susceptance respectively. The magnitudes of G and B are obtained from simulation. R_S is the series resistance of the device, g is the load conductance and L is the circuit inductance. L_p and C_p are the parasitic inductance and parasitic capacitance due to package respectively. The experimentally measured values of L_p and C_p for W-band package [15] is given in Table 2.

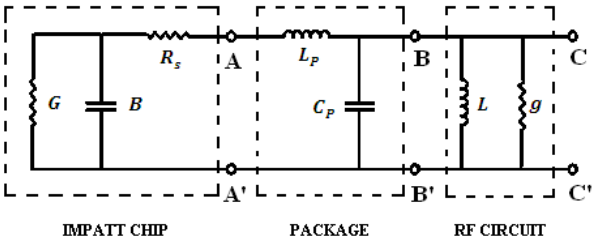

Figure 2: Equivalent model of the IMPATT source.

Device impedance across the ***AA***' terminal is given by,

$$Z_D = \left(\frac{1}{G + jB} + R_s\right) \tag{8}$$

Device-package combined impedance across the ***BB***' terminal is given by,

$$Z_{DP} = \left(Z_D + j\omega L_p\right) \left\| \left(\frac{1}{j\omega C_p}\right) = \left(\frac{1}{G + jB} + R_s + j\omega L_p\right) \right\| \left(\frac{1}{j\omega C_p}\right) \tag{9}$$

Impedance of the passive RF circuit,

$$Z_{RF} = \left[\frac{\left(\frac{1}{g}\right).j\omega L}{\left(\frac{1}{g}\right) + j\omega L}\right] \tag{10}$$

The conditions for stable oscillation are given by,

$$Real\left[Z_{DP} + Z_{RF}\right] = 0 \;\; \& \;\; Imaginary\left[Z_{DP} + Z_{RF}\right] = 0 \tag{11}$$

The values of negative conductance (*-G*) and susceptance (*B*) as functions of frequency can be obtained from the small-signal simulation method as described in the previous section. From those values of *-G* and *B* the overall device-package impedance as a function of frequency can be determined by using equation (11).

IV. RESULTS AND DISCUSSION

The DC parameters of the DDR Si IMPATT device designed and optimized to operate at *94 GHz* (Table 1) is obtained by using the double-iterative simulation technique [7] and listed in Table 3. Variation of breakdown voltage and DC to RF conversion efficiency with bias current density is shown in Figure 3. From Figure 3 it can be observed that the optimum bias current density for this device is obtained as 3.8×10^8 *Amp/m*^{2} for which the DC to RF conversion efficiency of the device is maximum.

The solutions of the equations (1) & (2) subject to the boundary conditions (3) & (4), i.e. the negative resistivity (*R(x)*) and reactivity (*X(x)*) profiles for different bias current densities are shown in Figure 4. *R(x)*-profiles shown in Figure 4 are characterized by two negative resistivity peaks in the two drift layers and central negative resistivity minimum located almost at the metallurgical junction. The negative resistivity peak in the electron drift layer is much larger in amplitude than the negative resistivity peak in the hole drift layer for the DDR Si IMPATT device. For Silicon, the reported experimental values of ionization rates of charge carriers [12] indicate the electrons have higher ionization rates than holes over a wide electric field range. Thus the relative amplitudes of the negative resistivity peaks in the two drift regions of DDR Si IMPTT device would depend on the values of ionization rates of charge carriers in the avalanche region of the device [16].

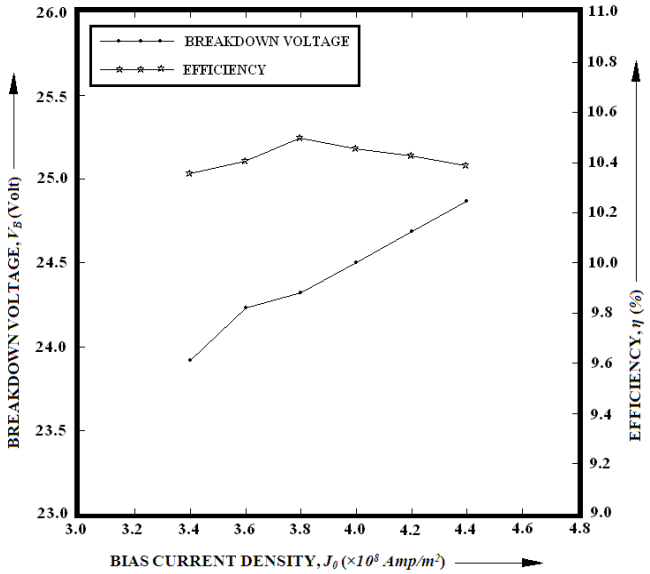

Figure 3: Variation of breakdown voltage and efficiency of the W-band DDR Silicon IMPATT device with bias current density.

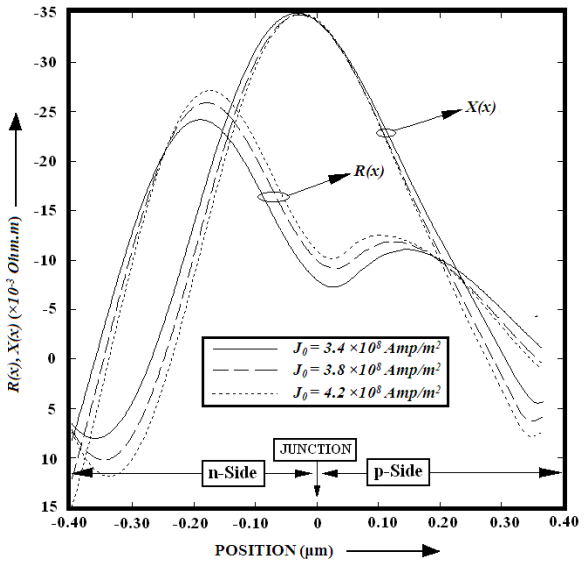

Figure 4: *R(x)* and *X(x)* profiles of the W-band DDR Silicon IMPATT device at different bias current densities.

Admittance characteristics i.e. the small-signal conductance-susceptance plots of the DDR Si IMPATT device without and with package for different bias current densities is shown in Figure 5 for an assumed series resistance of $R_s = 1.0\ \Omega$. It can be observed from Figure 5 that the magnitude of the negative conductance and peak optimum frequency of the device decreased significantly (*32.5 %* and *14.6 %* respectively for optimum bias current density of 3.8×10^8 *Amp/m*^{2}) due to the effect of package parasitics (i.e. L_p & C_p). Simulated small-signal parameters are listed in Table 4. From Table 4 it can be observed that the overall device-package *Q*-factor is degraded due the effect of package parasitics. RF power output decreased as the magnitude of the negative

conductance of the device decreased when the device is bonded into the package.

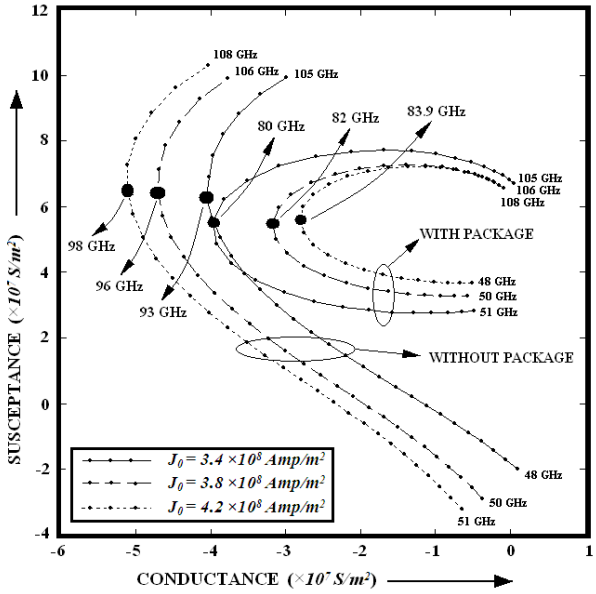

Figure 5: Admittance characteristics of the W-band DDR Silicon IMPATT device without and with package for different bias current densities (assuming, $R_s = 1.0\ \Omega$).

Variation of peak negative conductance and output RF power density of the packaged DDR Si IMPATT device with bias current density for different series resistance values is shown in Figure 6. Figure 6 shows that the effect of series resistance values on both the overall device-package negative conductance and output RF power density is prominent at the lower bias current densities; but it is not much significant at higher bias current densities.

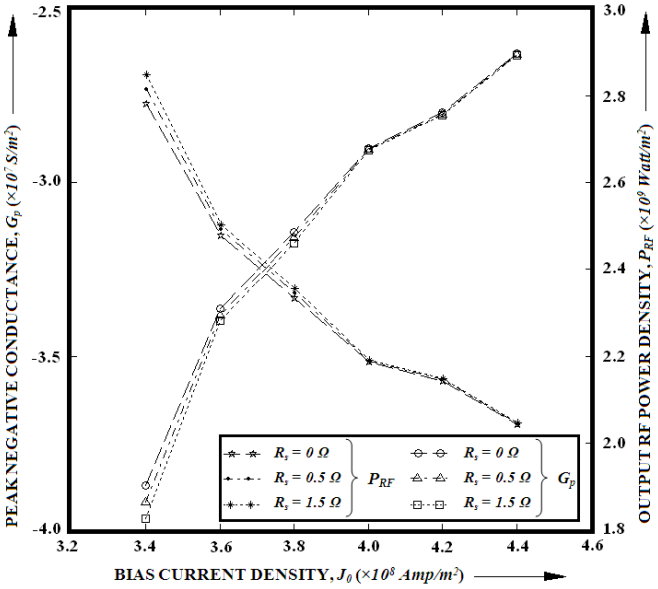

Figure 6: Variation of peak negative conductance and output RF power density of the W-band packaged DDR Silicon IMPATT device with bias current density for different series resistance values.

V. CONCLUSIONS

The effect of package parasitics on the mm-wave performance of DDR Si IMPATT device designed to operate at *94 GHz* window frequency is studied in this paper. Results show that the mm-wave performance of the device is degraded significantly when the device is bonded into the package. This investigation will be very much helpful to design and fabricate millimeter-wave DDR IMPATTs considering the effect of package parasitics.

TABLE 1: Design Parameters

BASE MATERIAL	DESIGN FREQUENCY, f_d (*GHz*)	*n*-EPITAXIAL LAYER THICKNESS, W_n (*μm*)	*p*-EPITAXIAL LAYER THICKNESS, W_p (*μm*)	*n*-EPITAXIAL LAYER DOPING, N_D ($\times 10^{23}\ m^{-3}$)	*p*-EPITAXIAL LAYER DOPING, N_A ($\times 10^{23}\ m^{-3}$)	SUBSTRATE LAYER DOPING, N_{Sub} ($\times 10^{26}\ m^{-3}$)
Silicon	94	0.400	0.380	1.200	1.300	1.000

TABLE 2: Package Parameters

FREQUENCY BAND	PACKAGE INDUCTANCE, L_p (*nH*)	PACKAGE CAPACITANCE, C_p (*pF*)
W-Band (*75 GHz - 110 GHz*)	0.05	0.13

TABLE 3: DC Parameters

SERIAL NUMBER	BIAS CURRENT DENSITY, J_0 ($\times 10^8$ *Amp/m²*)	PEAK ELECTRIC FIELD, ξ_m ($\times 10^7$ *Volt/m*)	BREAKDOWN VOLTAGE, V_B (*Volt*)	DC TO RF CONVERSION EFFICIENCY, η (%)	AVALANCHE WIDTH, x_A (*μm*)	x_A / W (%)
1	3.4	6.0293	23.92	10.35	0.350	44.87
2	3.6	6.0168	24.23	10.38	0.352	45.13
3	3.8	6.0043	24.32	10.49	0.354	45.38
4	4.0	5.9918	24.50	10.45	0.358	45.89
5	4.2	5.9793	24.69	10.42	0.362	46.41
6	4.4	5.9668	24.87	10.38	0.364	46.66

TABLE 4: Small-signal Parameters [$Rs = 1.0\ \Omega$]

SERIAL NUMBER	PEAK OPTIMUM FREQUENCY, f_p (*GHz*)		PEAK CONDUCTANCE, G_p ($\times 10^7$ *S/m²*)		PEAK SUSCEPTANCE, B_p ($\times 10^7$ *S/m²*)		QUALITY FACTOR, $Q = -(B_p/G_p)$		NEGATIVE RESISTANCE, Z_R ($\times 10^{-9}$ *Ohm/m²*)		OUTPUT RF POWER DENSITY, P_{RF} / A_j ($\times 10^9$ *Watt/m²*)	
	Without Package	With Package	Without Package	With Package	Without Package	With Package	Without Package	With Package	Without Package	With Package	Without Package	With Package
1	93	80.0	-4.0514	-3.9701	6.2720	5.5463	1.54	1.39	-7.2668	-8.5335	2.8978	2.8397
2	94	80.7	-4.4410	-3.3969	6.7061	5.2592	1.51	1.54	-6.8644	-8.6658	3.2312	2.4715
3	96	82.0	-4.7014	-3.1728	6.4215	5.4782	1.36	1.73	-7.4227	-7.9167	3.4749	2.3451
4	97	82.8	-4.9284	-2.9045	6.8341	5.8263	1.38	2.01	-6.9419	-6.8532	3.6992	2.1801
5	98	83.9	-5.1106	-2.8056	6.5009	5.5958	1.27	1.99	-7.4738	-7.1598	3.8946	2.1380
6	100	84.6	-5.2924	-2.6311	6.9339	5.9435	1.31	2.25	-6.9556	-6.2275	4.0948	2.0356

REFERENCES

[1] T. A. Midford and R. L. Bernick, "Millimeter Wave CW IMPATT diodes and Oscillators", IEEE Trans. Microwave Theory Tech., **27**, 483 (1979).

[2] Aritra Acharyya, Suranjana Banerjee and J. P. Banerjee, "Calculation of Avalanche Response Time for Determining the High Frequency Performance Limitations of IMPATT Devices", Journal of Electron Devices, **12**, 756 (2012).

[3] Aritra Acharyya, Suranjana Banerjee and J. P. Banerjee, "Dependence of DC and Small-signal Properties of Double Drift Region Silicon IMPATT Device on Junction Temperature", Journal of Electron Devices, **12**, 725 (2012).

[4] J. F. Luy, A. Casel, W. Behr and E. Kasper, "A 90-GHz double-drift IMPATT diode made with Si MBE," IEEE Trans. Electron Devices, **34**, 1084 (1987).

[5] Dalle C., Rolland P. and Lieti G. "Flat doping profile double-drift silicon IMPATT for reliable CW high power high-efficiency generation in the 94-GHz window", IEEE Trans Electron Devices, **37**, 227 (1990).

[6] S. M. Sze, and R. M. Ryder, "Microwave Avalanche Diodes", Proc. of IEEE, Special Issue on Microwave Semiconductor Devices, **59**, 1140 (1971).

[7] S. K. Roy, M. Sridharan, R. Ghosh, and B. B. Pal, "Computer method for the dc field and carrier current profiles in the IMPATT device starting from the field extremum in the depletion layer" in Proceedings of the 1st Conference on Numerical Analysis of Semiconductor Devices (NASECODE I), J. H. Miller, Ed. , Dublin, Ireland, 266 (1979).

[8] S. K. Roy, J.P. Banerjee and S. P. Pati, "A Computer analysis of the distribution of high frequency negative resistance in the depletion layer of IMPATT Diodes" in Proc. 4th Conf. on Num. Anal. of Semiconductor Devices (NASECODE IV), Dublin, Ireland (Dublin: Boole), 494 (1985).

[9] H. K. Gummel and J. L. Blue, "A small-signal theory of avalanche noise in IMPATT diodes", IEEE Trans. on Electron Devices, **14**, 569 (1967).

[10] M. Sridharan and S. K. Roy, "Computer studies on the widening of the avalanche zone and decrease on efficiency in silicon X-band sym. DDR", Electron Lett., **14**, 635 (1978).

[11] M. Sridharan and S. K. Roy, "Effect of mobile space charge on the small signal admittance of silicon DDR", Solid State Electron, **23**, 1001 (1980).

[12] W. N. Grant, "Electron and hole ionization rates in epitaxial Silicon", Solid State Electron, **16**, 1189 (1973).

[13] C. Canali, G. Ottaviani and A. A. Quaranta, "Drift velocity of electrons and holes and associated anisotropic effects in silicon", J. Phys. Chem. Solids, **32**, 1707 (1971).

[14] "Electronic Archive: New Semiconductor Materials, Characteristics and Properties," http://www.ioffe.ru/SVA/NSM/Semicond.

[15] G. M. Brooker, "Long-range Imaging Radar for Autonomous Navigation", Ph.D. dissertation, University of Sydney. Aerospace, Mechanical and Mechatronic Engineering, 231 (2006).

[16] J. P. Banerjee, S. P. Pati and S. K. Roy, "High frequency characterisation of double drift region InP and GaAs diodes", Appl. Phys. A, **48**, 437 (1989).